Lawrence Berkeley National Laboratory

LBL Publications

Title

Dynamics of hydride anion and acetyloxyl radical production by electron attachment to acetic acid

Permalink

https://escholarship.org/uc/item/2kw9h9f6

Journal

The Journal of Chemical Physics, 161(16)

ISSN

0021-9606

Authors

Hasan, M

Weber, Th

Centurion, M

et al.

Publication Date

2024-10-28

DOI

10.1063/5.0226252

Peer reviewed

eScholarship.org Powered by the California Digital Library
University of California

ACCEPTED MANUSCRIPT
The Journal of Chemical Physics
AIP Publishing
This is the author's peer reviewed, accepted manuscript. However, the online version of record will be different from this version once it has been copyedited and typeset.
PLEASE CITE THIS ARTICLE AS DOI: 10.1063/5.0226252

Dynamics of hydride anion and acetyloxyl radical production by electron attachment to acetic acid

M. Hasan,[1,2] Th. Weber,[1] M. Centurion,[2] and D. S. Slaughter[1]
[1)]*Chemical Sciences Division, Lawrence Berkeley National Laboratory, Berkeley, CA 94720, USA*
[2)]*Department of Physics and Astronomy, University of Nebraska-Lincoln, Lincoln, Nebraska 68588, USA*

(*Electronic mail: DSSlaughter@lbl.gov)

(Dated: 1 October 2024)

We investigate the dynamics and site-selectivity in the dissociation of transient anions formed upon attachment of low energy electrons to acetic acid by anion fragment momentum imaging experiments. The resonances at 6.7 eV and 7.7 eV are confirmed to dissociate exclusively by the O-H bond, while a third resonance at 9.1 eV dissociates primarily by both C-H break O-H break. A fourth resonance near 10 eV is found to dissociate by O-H break. For each resonance, the measured kinetic energy release indicates 2-body dissociation produces a neutral radical in the ground electronic state, for all four resonances. The measured angular distributions are consistent with all four resonances having A' symmetry.

I. INTRODUCTION

Simple carboxylic acids are well established to exhibit rich chemical reactivity in environments that are exposed to low energy free electrons[1]. Dissociative electron attachment (DEA) is an important reaction that occurs by resonant electron-molecule interactions, producing a transient negative ion (TNI) resonance[2]. There are many prominent examples of molecules having several anion resonances, characterized as single-electron shape resonances, or excited resonances, where a target electron is excited in the electron attachment process, producing a correlated two-electron one-hole system that decays by autodetachment or dissociation[3]. Feshbach resonances occur when the potential energy of the anion resonance is lower than the corresponding excited state of the neutral molecule. This energetically forbids the resonance from decaying by single-electron autodetachment, thus enabling nuclear motion and dissociation to proceed on femtosecond timescales.

Acetic acid produces several reactive anions and neutral radicals by DEA, which proceeds via a shape resonance at low attachment energies below 3 eV, or via Feshbach resonances at higher energies above 5 eV[4–8]. Sailer *et al.*[4] reported nine fragment anions in the 0-13 eV electron energy range with the dominant products being $CH_2O_2^-$ and CH_3COO^-, appearing from two low energy resonances at 0.75 eV and 1.5 eV, respectively. They also performed *ab initio* calculations and assigned these states as single particle shape resonances to the two lowest unoccupied molecular orbitals, LUMO and LUMO+1. Subsequent works in Refs.[5,6] confirmed the existence of a 1.5 eV shape resonance in the dissociation channel producing CH_3COO^-. Freitas *et al.*[9] performed electronic structure calculations using the Schwinger multichannel method and found that the π^* shape resonance at 1.5 eV is characterized by single occupation of the LUMO, having A'' symmetry, with dissociation enabled by nonadiabatic coupling to an A' state. They found no explanation for the lower energy production of $CH_2O_2^-$ that was reported in the experiments of Sailer *et al.*[4,5]. Recently, Chakraborty *et al.*[7] reported a velocity slice imaging study of the heavier anion fragments around the 10 eV Feshbach resonance, tentatively assigning the $13a'$ Rydberg state as the parent TNI state by comparing the resonance energy with the $13a'' \rightarrow 3pa''$ Rydberg transition that was reported at 9.268 eV in vacuum ultraviolet (VUV) photoabsorption spectroscopic studies by Leach *et al.*[10].

Prabhudesai *et al.*[11,12] carried out DEA measurements leading to H^- ions from acetic acid, and H^- and D^- from partially deuterated acetic acid, CH_3COOD, in the energy range of 0-18 eV identifying three resonance peaks. For CH_3COOD, they found that the first two sharp resonances at 6.7 eV and 7.7 eV contributed to the O-D bond break, and the third broad resonance, centered at 9.1 eV, produced H^- by C-H bond break. The relative yields of H^- and D^- from two different bond scissions confirmed the existence of a functional group dependence leading to site-selective fragmentation at the hydrogen site, which was also observed in condensed phase acetic acid[13]. Despite H^- being the dominant anion fragment around 6-10 eV from DEA to acetic acid[11,12], the resonance symmetries, dissociation mechanisms, and the dynamics of the TNI resonances in acetic acid remain poorly understood.

Dissociation of acetic acid by O-H break produces H^- and an acetyloxyl radical, CH_3COO, which has several low-lying excited electronic states[14,15] that could be significantly populated at ambient temperatures. This radical is therefore an important intermediate in atmospheric, combustion, and synthetic organic chemistry[16,17]. Dissociation by C-H break results in a carboxymethyl radical, CH_2COOH, which may play an important role in the formation of glycine and other complex organic molecules in planetary atmospheres and interstellar media[18].

In this work we focus on the rich information provided by the momentum distributions of either H^- or D^- anions, produced by breaking specific bonds, namely the hydroxyl (O-H or O-D) and/or methyl (C-H or C-D) bonds, such that the structure of the radical fragment is determined by the resonance energy. For this, we have carried out anion fragment momentum imaging measurements on acetic acid

ACCEPTED MANUSCRIPT
The Journal of Chemical Physics
AIP Publishing
This is the author's peer reviewed, accepted manuscript. However, the online version of record will be different from this version once it has been copyedited and typeset.
PLEASE CITE THIS ARTICLE AS DOI: 10.1063/5.0226252

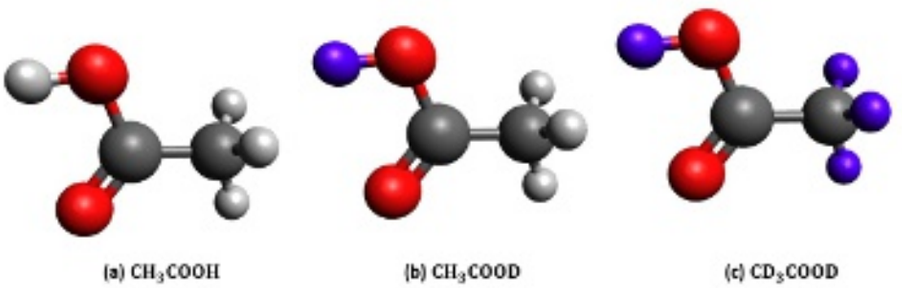

FIG. 1. Molecular structure of (a) acetic acid, (b) partially deuterated acetic acid, and (c) fully deuterated acetic acid.

(CH_3COOH) partially deuterated acetic acid, CH_3COOD, and fully deuterated acetic acid (CD_3COOD), their structural schematics shown in Fig. 1. We examine the kinetic energy and angular distributions of the H^- and D^- fragments measured by 3D anion fragment momentum imaging in the 6.7 eV to 10 eV energy range. Anion fragment angular distributions contain information about the symmetry of the resonance states as well as the associated dissociation dynamics of the specific dissociation channel of interest.

We continue with a brief description of the experimental technique in Sec. II. In Sec. III, we describe a model that we employ to analyze the experimental angular distributions to understand the possible resonance symmetries. In Sec. IV, we summarize our experimental results for the O-H and C-H bond breakage that are provided by momentum images as well as the associated kinetic energy and angular distributions. In Sec. V and VI, we discuss the results and provide concluding remarks.

II. EXPERIMENTAL SETUP

The experimental apparatus used in the present study has been described in detail previously in Ref.[19]. Here we provide a brief discussion of the experimental arrangement most relevant to the current work. Briefly, the setup consists of an ultra-high vacuum chamber, housing an energy-tunable pulsed electron beam from a commercially acquired electron gun (Kimball Physics Inc.) and an effusive gas jet of the molecular target from a stainless steel capillary that was directed perpendicular to the electron beam. The gun produces 80 ns pulses of electrons at 50 kHz repetition rate, with an energy spread of 0.5 eV full-width-at-half-maximum in a beam 1 mm in diameter.The molecular target sample is evaporated from a glass sample holder, outside of the vacuum chamber, and the vapor is guided by heated tubing to a feedthrough into the vacuum chamber and the capillary. The tubing and capillary are heated to approximately 80° C. A pair of Helmholtz coils, producing a 25 G uniform magnetic field coaxial to the electron beam, collimates and transports the electrons to the interaction region while preventing most of any scattered electrons from entering the anion imaging spectrometer. The anion yields of O^- from DEA to CO_2 across the thermodynamic threshold at 3.99 eV were measured for the calibration of the electron beam mean energy, which was checked before and after each experiment.

The 3D anion fragment momentum imaging spectrometer consists of a series of copper electrodes that constitutes an ion acceleration region and an ion focusing drift region, with the time-of-flight direction being orientated perpendicular to the electron beam and parallel to the effusive gas jet direction. An ion repeller electrode is grounded while the electron beam packet passes through the interaction region. It is then subsequently pulsed to -35 V, in order to push any anions formed in the electron-molecule attachment process into the spectrometer, after the short electron bunch (80 ns) cleared the interaction region. In the present experiments, the electric field was typically 24 V/cm over the entire acceleration region. In the ion focus region of the spectrometer, which forms an electro-optical lens to compensate for the extended electron-molecule interaction volume, the electric field was varied from 120 V/cm to 0 V/cm. The anions are momentum-imaged onto a pair of time sensitive 80 mm diameter multichannel plates chevron stack, equipped with a position-sensitive delay-line anode. The arrival times and positions of the ions were recorded event-by-event in list-mode format. After a thorough off-line calibration and analysis, the 3D momenta of each ion fragment were generated. A momentum calibration was performed by measuring the well-known O^- kinetic energy and angular distributions from DEA to O_2[20,21]. The accuracy of the momentum calibration was confirmed by inspection of the H^- and O^- kinetic energies and momentum images of background water[22] and CO_2[23], at electron attachment energies of 6 eV and 8 eV, respectively.

The H^- channel can be formed by hydroxyl (O-H) or methyl (C-H) bond break. The dissociation channels were isolated by performing experiments with acetic acid deuterated only at the hydroxyl site (CH_3COOD). The anion imaging spectrometer allows us to identify H^- and D^- by their times-of-flight, and thus the contributions of each dissociation channel at different energies were separated. The thermodynamic thresholds for the relevant two-body and three-body reactions are given in Tab. I. Due to the absence of electron and molecular beam monitoring and stabilization in the present experi-

ACCEPTED MANUSCRIPT
The Journal of Chemical Physics
AIP Publishing
This is the author's peer reviewed, accepted manuscript. However, the online version of record will be different from this version once it has been copyedited and typeset.
PLEASE CITE THIS ARTICLE AS DOI: 10.1063/5.0226252

ments, we cannot compare the ion yields between different experiments to provide information on the absolute DEA cross sections. The purity of each acetic acid sample was specified by the supplier at $\geq$ 98.5%, <1% water for CH_3COOD, $\geq$ 99.5% for CD_3COOD, and $\geq$ 99.9985% for CH_3COOH. Each sample was degassed by several freeze-pump-thaw cycles after loading it in the sample holder.

III. ANGULAR DISTRIBUTIONS

In the axial recoil approximation (ARA)[29], the dissociation axis of a molecule does not rotate significantly during the dissociation process, i.e., the dissociation of the TNI state occurs much faster than the rotation of the bond, proceeding either by molecular rotation or other nuclear degrees of freedom. Consequently, the angular dependence of electron attachment in the molecular frame is preserved in the dissociation as long as the ARA is valid. A result of the ARA is the angular distribution fragment ions, with respect to the incoming electron beam direction, depends only on the electron attachment probability in the body-fixed frame of the molecule[30,31]. Within the ARA, the fragment angular distributions can reveal the electronic symmetry or nuclear conformation of the initial state[32,33]. In some previous studies, electron scattering theory has been employed to predict fragment angular distributions under the ARA and, when compared with anion fragment imaging measurements, the ARA was found to break down, indicating coupled electronic and nuclear dissociation dynamics[34] and conical intersections[35] coupling electronic states of the anion.

O'Malley and Taylor[30] pioneered early theory efforts to connect the fragment angular distribution to the symmetry of the resonance states of the transient anions produced in DEA. This theory applies specifically to diatomic molecules and assumes that (i) only a single electronic state contributes to a DEA resonance and, (ii) that the subsequent dissociation obeys the ARA, i.e., that the negative ion state does not undergo a rotation during the dissociation, and (iii) that the coupling is independent of the spin states, i.e., only depends on pure electronic matrix elements. Using the above approximations, Azria *et al.*[36] later expanded this theory to polyatomic molecules and obtained the following expression for the distribution of the anionic fragments as a function of the angle θ relative to the incident electron beam:

$$I^{\varepsilon}(\theta) \propto \frac{1}{2\pi}\int_0^{2\pi} |\sum_{lm} a_{lm} i^l e^{i\delta_l} \chi^{\varepsilon}_{lm}(\theta,\phi)|^2 d\phi \qquad (1)$$

where (θ,ϕ) are the polar and azimuthal angles between the electron beam and the dissociation axis of the anion. $\chi^{\varepsilon}_{lm}(\theta,\phi)$ are the basis functions of the irreducible representation of the point group of the molecule and are expressed in terms of a linear combination of spherical harmonics in the molecular dissociation frame. The expansion coefficients a_{lm} are real numbers. The phases δ_l represent the contributions of the direct scattering process to the DEA resonance[37]. The values of the indices l and m with a non-zero contribution to the sum in Eq. (1) are restricted to the irreducible representation of the resonant state. Only a few values of partial waves, for instance up to $l = 2$, where $l = 0, 1$ and 2 represent s, p and d partial waves, respectively, are needed to fit the angular distributions. As the number of partial waves increases, so does the number of maxima and minima in the angular distributions[36].

The application of this model to fit the experimentally measured angular distributions has been demonstrated for several diatomic[37] and polyatomic molecules[36,38–42]. The applicability of this approach is limited to single resonance cases only, and the coupling of two resonances may not be treated properly.More rigorous methods require *ab initio* electron scattering calculations[34]. However,such calculations are computationally expensive, even for small molecules, and require an extensive survey of the electron-molecule autodetachment continuum to identify the most relevant states, which is beyond the scope of the present experimental study.

Acetic acid, in the equilibirum geometry of the ground electronic state, is planar with the symmetry point group C_s. The C_s point group has two symmetry operations: identity, E, and reflection through the mirror plane, σ_h. The two symmetries in the two irreducible representations associated with the Cs point group are A' and A''. The A' representation is symmetric to both E and σ_h. The A'' representation is symmetric to E but antisymmetric to σ_h. The ground state configuration of acetic acid, according to the density functional theory molecular orbital calculations of Leach *et al.* [10], is $(1a'-10a')^2(1a'')^2(11a')^2(12a')^2(2a'')^2(3a'')^2(13a')^2$, which has A' symmetry. The angular distribution function under the ARA for $A' \rightarrow A'$ transitions with the three lowest partial waves s,p and d, is

$$\begin{aligned} I^{A'}(\theta) =& \alpha_{00}^2 + 2\alpha_{00}\alpha_{10}\sin(\delta_0-\delta_1) \\ &+ \alpha_{10}^2\cos^2(\theta) + \alpha_{11}^2\sin^2(\theta) + \alpha_{20}^2(3\cos^2(\theta-1)^2 \\ &+ \alpha_{21}^2\cos^2(\theta)\sin^2(\theta) + \alpha_{22}^2\sin^4(\theta) \\ &+ 2\alpha_{00}\alpha_{20}\cos(\delta_0-\delta_2)(3\cos^2(\theta-1)^2 \\ &+ 2\alpha_{10}\alpha_{20}\sin(\delta_1-\delta_2)\cos\theta(3\cos^2(\theta-1)^2 \\ &+ 2\alpha_{11}\alpha_{21}\sin(\delta_1-\delta_2)\cos\theta\sin^2(\theta) \end{aligned} \qquad (2)$$

and the $A' \rightarrow A''$ transitions, with the two lowest partial waves p and d is

$$\begin{aligned} I^{A''}(\theta) =& \alpha_{11}^2\sin^2(\theta) + \alpha_{21}^2\sin^2(\theta)\cos^2(\theta) + \alpha_{22}^2\sin^4(\theta) \\ &+ 2\alpha_{11}\alpha_{21}\sin(\delta_1-\delta_2)\cos\theta\sin^2(\theta) \end{aligned} \qquad (3)$$

In the following Section we fit the measured angular distributions with Equations (2) and (3) to find the resonance symmetry.

IV. RESULTS

The experimental results are organized as follows. We present the momentum imaging experimental results obtained from the dissociation products of the O-H/O-D and C-H/C-D bond breakages of acetic acid and its partially- and fully-deuterated isotopologues, over the energy range 6.7 eV to

ACCEPTED MANUSCRIPT
The Journal of Chemical Physics
AIP Publishing
This is the author's peer reviewed, accepted manuscript. However, the online version of record will be different from this version once it has been copyedited and typeset.
PLEASE CITE THIS ARTICLE AS DOI: 10.1063/5.0226252

TABLE I. Energetics of various dissociation channels producing H^- fragments. The enthalpy of formation, bond energies, and electron affinities were taken from Refs.[12,24–28]

Number	Dissociation channel	Thermodynamic threshold (eV)
1	$H^- + CH_3COO$	4.02
2	$H^- + CH_2COOH$	3.47
3	$H^- + CH_3 + CO_2$	3.39
4	$H^- + CH_2CO + OH$	5.46
5	$H^- + CH_2 + COOH$	7.99

10 eV. We then present the ion kinetic energy distributions, which we extract directly from the measured absolute momenta. Finally, we present the angular distributions and, following the procedure discussed in section III, we fit our angular distributions for the candidate $A' \rightarrow A'$ and $A' \rightarrow A''$ transitions to determine the symmetry of the TNI state.

A. H^- (D^-) due to O-H (O-D) bond break

The measured momentum images of the D^- anions resulting from DEA to partially deuterated acetic acid, CH_3COOD, at the first resonance (6.7 eV) are displayed in Fig. 2a. For each momentum image, the entire 3D momentum distribution of H^-/D^- ions is projected onto the longitudinal and transverse momentum coordinates with respect to the incident electron beam direction. The longitudinal and transverse coordinates are parallel and perpendicular to the incident electron beam, respectively.In Fig. 2a, a minor contribution due to the presence of $< 1\%$ D_2O in the sample is visible around longitudinal momentum = 0 and |transverse momentum| $<$ 20 a.u. The main circular feature corresponds to D^- from CH_3COOD. We note, for electron attachment energies above 6.7 eV, the DEA cross section to produce D^- from D_2O decreases rapidly to values 5- to 10-fold smaller[43], and we observe no significant contributions from water above 6.7 eV. We observe that the momentum distributions of the D^- from CH_3COOD have comparable intensity in the forward (positive longitudinal) and perpendicular directions, while exhibiting maximum intensities in the backward (negative longitudinal) direction. The transformation of the 3D momentum distributions to longitudinal and transverse coordinates[19] projects uncertainties at very small transverse momenta, which we see as noise along zero transverse momentum.

The momentum distribution of D^- from CH_3COOD (Fig. 2b) at the second resonance (7.7 eV) shows a similar maximum in the backward direction just like the first resonance at 6.7 eV. In contrast to the momentum image at 6.7 eV, the 7.7 eV momentum image has broader peaks in the backward and perpendicular directions. As the electron energy is increased to 9.1 eV in Fig. 2c, we observe a similar structure again, with a maximum ion yield in the backward and perpendicular directions and with very little ion yield in the forward direction. Fig. 2d shows the momentum distribution of the D^- ions from CH_3COOD at 10 eV, where two distinct rings, corresponding to two different ion momenta, i.e., fast and slow ions, are observed, indicating two different dissociation pathways. The outer ring (fast D^-) and inner ring (slow D^-) have momenta of $\approx$ 27 a.u. and $\approx$ 35 a.u., respectively. The ion emission patterns of the fast and slow ions have similar features: a global maximum in the backward direction, and significant yields in the perpendicular and forward directions. We note that the ion yield of the slow D^- appears to be smaller than the yield for the fast D^- at 10 eV, however the relative yields depend strongly on the incident energy, and are almost equal at 9.6 eV.

The kinetic energy distributions of the D^- ions, obtained from DEA to CH_3COOD, are shown in Fig. 3. The kinetic energy distribution of D^- at 6.7 eV (solid black curve) has two features: a peak at 2.39 eV, and a low-energy shoulder around 1.6 eV. Previous studies[22,43,44] showed that the cross-sections for producing H^- and D^- from DEA to H_2O and D_2O, respectively, is very high at 4.6 $\times 10^-18$ cm^2 around 6.7 eV. Therefore, any D^- fragments from DEA to D_2O contaminants are expected to be strongest around this energy. The kinetic energy for the 1.6 eV feature is consistent with a small ($< 1\%$) contamination of the CH_3COOD sample with D_2O[22]. We also performed H^- DEA momentum imaging measurements at the 6.7 eV and 7.7 eV resonances in CH_3COOH and D^- from CD_3COOD, neither of which are presented here, because the water contamination in each sample was evidently higher, such that the $H^-(D^-)$ contribution from DEA to background H_2O (D_2O) was more significant. Any contributions from H_2O and D_2O at energies higher than 7 eV were determined, by the same comparisons, to be insignificant.

The 2-body dissociation producing D^- anions by O-D bond cleavage can be written in the form of Reaction 1 in Tab. I. Based on the thermochemical data[12,24,25], the threshold for this dissociation channel is 4.02 eV. The difference between the incident energy and the threshold for the reaction to take place is the excess energy, which is 2.68 eV for an incident electron energy of 6.7 eV. This energy is distributed between the translational kinetic energies and the internal energies of the fragments. Using momentum conservation, we can estimate the total kinetic energy release, E_T:

$$E_T = E_T^i \times \frac{M}{m} \tag{4}$$

where, E_T^i, M, and m are the kinetic energy of the D^- fragment, the mass of the parent molecule, CH_3COOD, and the

ACCEPTED MANUSCRIPT
The Journal of Chemical Physics
AIP Publishing
This is the author's peer reviewed, accepted manuscript. However, the online version of record will be different from this version once it has been copyedited and typeset.
PLEASE CITE THIS ARTICLE AS DOI: 10.1063/5.0226252

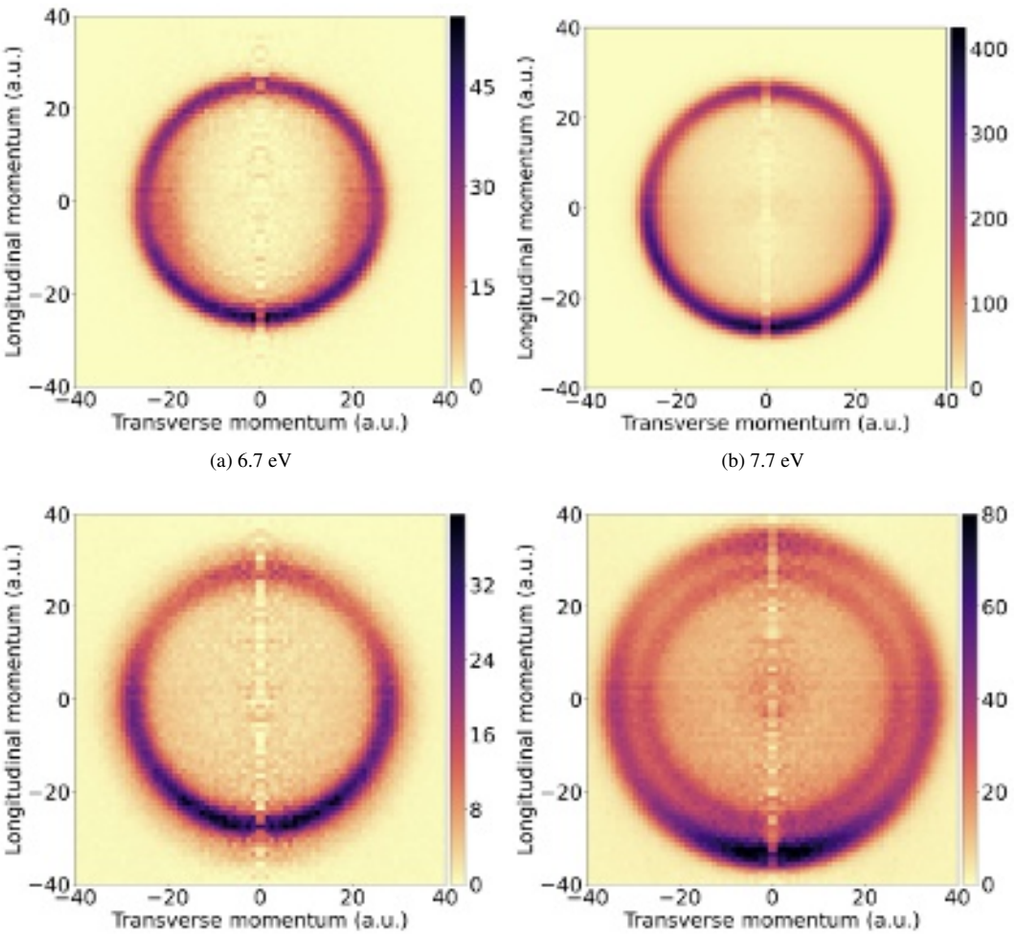

(a) 6.7 eV (b) 7.7 eV

(c) 9.1 eV (d) 10 eV

FIG. 2. Momentum distribution of D^- ions from O-D bond cleavage of CH_3COOD at incident electron energies of 6.7, 7.7, 9.1 and 10 eV. The incident electron momentum is in the positive longitudinal direction (upward), and each color scale shows the ion yield in arbitrary units.

mass of the neutral fragment, CH_3COO, respectively. At the incident electron energy of 6.7 eV, the peak in the kinetic energy distribution is 2.39 eV. The difference between the excess energy and E_T is 0.25 eV. This is 9% of the available excess energy, and it contributes to rotational and/or internal excitation of the CH_3COO fragment. At 7.7 eV, the kinetic energy of the D^- anion has a peak at 2.6 eV, corresponding to $E_T = 2.69$ eV. The excess energy is 3.68 eV, leaving about 27% of the available excess energy as rotational or internal energy in the neutral molecular fragment. As the incident electron energy is increased to 9.1 eV at the 3rd resonance in Fig. 3 for D^-/CH_3COOD, about 2.1 eV (corresponding to 41% of the excess energy) goes into the internal energy of the neutral fragment. At 10 eV, the peak corresponding to the slow D^- is similar in energy and width to the peak at 9.1 eV. In contrast, the fast D^- kinetic energy peak is at 4.5 eV, and the width of the fast D^- distribution is about 2 eV. About 1.52 eV and 2.9 eV (i.e., $\approx$ 25% and 48% of the excess energy) is partitioned into rotational or internal excitation of the fast and slow neutral fragments, respectively. Remarkably, for all of the incident energies in the present experiments, more than 50% of the dissociation energy is partitioned into the translational energy of the dissociating fragments.

Fig. 4a shows the angular distribution of the D^- ions from O-D bond breakage for the first resonance at 6.7 eV from DEA to CH_3COOD. Here, we include only the ions with kinetic energies above 1.8 eV, in order to exclude any possible contributions from the small background of D_2O. The dissociation angle is defined with respect to the incident electron beam direction. Most of the fragment ion yield is in the backward direction $> 120°$, with smaller ion yields in the range of $0-120°$. The measured angular distributions are fitted with equations (2) and (3), for three models: (i) $s+p(A')$ (blue),(ii) $s+p+d(A')$ (black), and (iii) $p+d(A'')$ (purple). The angular distributions clearly show a finite ion yield in the 0° and 180° directions (i.e., parallel and antiparallel to the electron beam, corresponding to right and left in Fig. 4a), requiring an s-wave contribution. Consistently, the fit with partial waves $p+d$ corresponding to an $A' \rightarrow A''$ transition model shows the poorest agreement with the experimental data. The fit with only the

ACCEPTED MANUSCRIPT
The Journal of Chemical Physics
AIP Publishing
This is the author's peer reviewed, accepted manuscript. However, the online version of record will be different from this version once it has been copyedited and typeset.
PLEASE CITE THIS ARTICLE AS DOI: 10.1063/5.0226252

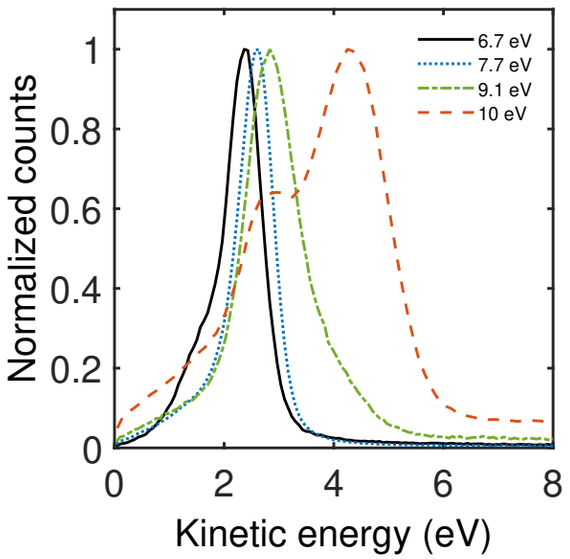

FIG. 3. Kinetic energy distribution of D^- ions from O-D bond cleavage of CH_3COOD at incident electron energies of 6.7, 7.7, 9.1 and 10 eV. The ion yield for each distribution is rescaled to a maximum of 1 (arbitrary units).

two lowest partial waves $s+p$ ($A' \rightarrow A'$) fails to reproduce the forward-backward asymmetry in the measured angular distributions. The addition of a d-wave to $s+p$, in the $s+p+d(A')$ model, reproduces the profile of the of the angular distribution much better at all angles with an $R^2 \approx 0.96$. This clearly indicates that at 6.7 eV, the populated TNI state has A' symmetry, if we assume that the ARA holds.

The measured angular distributions of the D^- ions at 7.7 and 9.1 eV from DEA to CH_3COOD, corresponding to the second and third resonances, respectively, are shown in Figs. 4b-4c. The two resonances have qualitatively similar angular distributions of the D^- ions, which peak around 100° and 170° with a shallow minimum around 50° and a small local maximum around 0°. These features contrast with the lower energy resonance (Fig. 4a), which is generally more isotropic. Both, the 7.7 eV and 9.1 eV angular distributions are consistent with $s+p+d$ ($A' \rightarrow A'$) transition models (black curves in Figs 4b-4c), which produce satisfactory fits with $R^2 \approx 0.99$. In contrast, the $p+d(A'')$ and $s+p(A')$ transition models fit the experimental data poorly, failing to produce the measured maxima or relative forward and backward ion yields. Therefore, it is most plausible that both the 7.7 and 9.1 eV resonances have A' symmetry under axial recoil approximation.

For 10 eV electron attachment, we examine the fast and slow ions in Figs. 4d and 4e, respectively. In both cases, the preferred general direction of ion ejection is again in the backward direction, opposite to the incident electron beam. Again, only the model including the lowest three partial waves $s+p+d$ ($A' \rightarrow A'$) provides a satisfactory fit, $R^2 > 0.97$, strongly suggesting that the 10 eV resonance also has A' symmetry.

B. $H^-(D^-)$ due to C-H (C-D) bond break

The momentum images of the H^- and D^- anions for the C-H/C-D bond break from the third resonance at 9.1 eV for DEA to CH_3COOH, CH_3COOD, and CD_3COOD are shown in Figs. 5a-c. Besides the faster H^-/D^- ions (outer rings in Figs. 5a-c), slower ions are also observed at the center of the image in each case. The ion yields of the fast H^-/CH_3COOH breakups are generally highest in the perpendicular, forward, and backward directions. The slow H^- anions from DEA to CH_3COOH and CH_3COOD appear to be ejected almost isotropically, with a weak maximum in the perpendicular directions. In contrast, the slow D^- ions from DEA to CH_3COOD show a similar structure as the fast ions. The kinetic energy distributions for the C-H (C-D) break show two distinctive peaks, corresponding to the outer peak (fast H^-/D^- ions) and the inner peak (slow ions) inFig. 6. This general structure is exhibited by all three isotopologues in the present experiments. The pathway for C-H bond cleavage can be represented by Reaction 2 in Tab. I, with a thermodynamic threshold of 3.47 eV. The slow H^-/D^- ion peaks occur at about 1 eV, indicating that about 4.6 eV (corresponding to $\approx$ 82% of excess energy) is partitioned to excitation or few-body dissociation of the neutral fragment(s). The peak kinetic energy of the fast ions are 3.65, 4.45, and 3.35 eV for the H^-/CH_3COOH, H^-/CH_3COOD, and D^-/CD_3COOD channels, respectively. The internal energy of each neutral fragment is in the range of 1.15 to 2.28 eV, corresponding to 20% to 40% of the excess energy.

We now consider H^- from 9.1 eV DEA to CH_3COOH (Fig. 5a), which, by comparison with Fig. 2c, clearly occurs mostly by C-H break. Fig. 7a shows the angular distributions of the fast (3.6 eV to 4.6 eV) H^- ions for this attachment energy. The distribution of Fig. 7a has a maximum around 90°, two shallow minima around 45° and 125°, and significant yields at 0° and 180°. Applying the $s+p+d(A')$ model (black curve) gives a reasonable fit to the measured distribution, with an R^2 value of 0.8. In contrast, the $p+d(A'')$ model (dotted purple curve) fails to capture the measured ion yield in the forward and backward directions, and the $s+p(A')$ model (dashed blue curve) fails to capture the forward-backward asymmetry . This suggests that the 9.1 eV resonance has A' symmetry. Similar features are also observed in angular distributions for fast H^- and D^- ions from CH_3COOD and CD_3COOD in Figs. 7c and 7e, which are each in good agreement with $s+p+d(A')$ model fits (black curves in Figs7e).

V. DISCUSSION

To understand the dynamics of DEA to acetic acid, we consider the possible symmetries of the resonances, the measured angular distributions, and the possible final states of the dissociation products. First, we discuss the ground and low lying excited vibrational and electronic states of the dissocia-

ACCEPTED MANUSCRIPT
The Journal of Chemical Physics
AIP Publishing
This is the author's peer reviewed, accepted manuscript. However, the online version of record will be different from this version once it has been copyedited and typeset.
PLEASE CITE THIS ARTICLE AS DOI: 10.1063/5.0226252

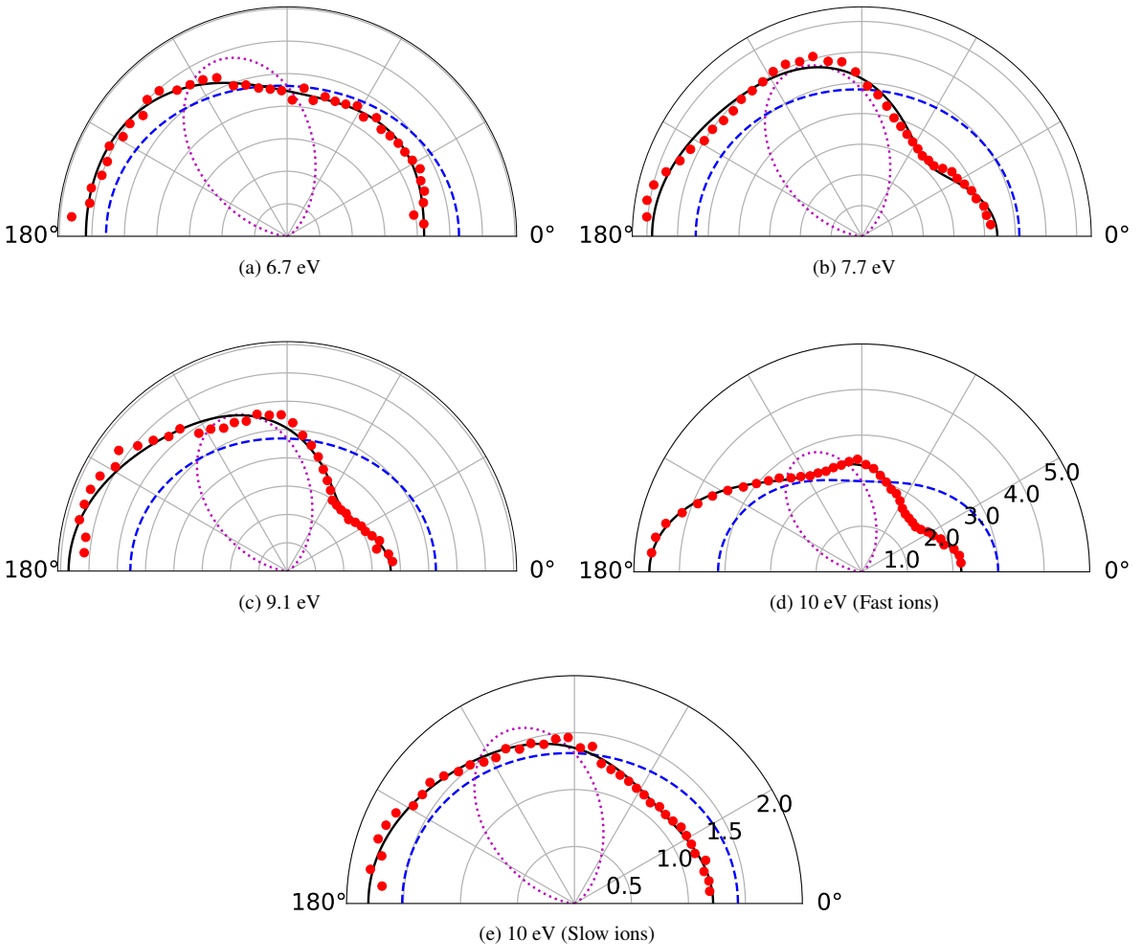

(a) 6.7 eV (b) 7.7 eV (c) 9.1 eV (d) 10 eV (Fast ions) (e) 10 eV (Slow ions)

FIG. 4. Angular distributions of D^- ions from O-D bond cleavage of CH_3COOD, at 6.7, 7.7, 9.1 and 10 eV. The experimental angular distributions (solid red circles) are fitted assuming $A' \rightarrow A'$ transitions using partial waves s+p (dotted blue lines) and s+p+d (solid black line), and under the assumptions of $A' \rightarrow A''$ transitions using partial waves p+d (dotted purple lines). The incident electron direction is 0 deg,and the ion yields are displayed on a linear scale in arbitrary units.

tion products and their stability with respect to energy absorption, identify the possible dissociation pathways in the three resonance regions. Next, we compare our results with the VUV photoabsorption and electron energy loss (EELS) spectra of neutral acetic acid available in the literature. Finally, we consider the possible electron attachment probabilities in the molecular frame (the entrance amplitude), within the axial recoil approximation, for acetic acid by comparing with the well studied Feshbach resonances in formic acid.

Photodetachment and photoelectron-photofragment coincident spectroscopy[15] were employed to study the dissociation dynamics of the neutral acetyloxyl radical, CH_3COO, starting from the acetate anion (CH_3COO^-) equilibrium geometry. A stable neutral radical (CH_3COO or CH_2COOH) and dissociation products CH_3 and CO_2, were found following photodetachment. The branching ratio of 1:9 between the generation of a stable radical and a dissociation suggested that CH_3COO is metastable and undergoes spontaneous uni-molecular dissociation, rather than direct dissociative photodetachment. The study also found that the fragment CH_2COOH is the result of an isomerization process of CH_3COO after photodetachment. The exact path for hydrogen atom transfer is not known, but it was found to be energetically favorable[45,46] with a barrier height of 0.08 eV between the lowest states of CH_3COO and CH_2COOH. The lowest few electronic states of the acetyloxyl have also been studied computationally. The ground electronic state has been characterized as a B_2-like $^2A''$ state, and the lowest excited electronic state was found to be only 0.1 eV to 0.2 eV higher in energy having $^2A'$ character[14]. The second excited electronic state is predicted to be about 0.7 eV above the ground state[47]. High-resolution photoelectron imaging of acetate anions[48] found two bound vibrational states around 0.048 eV and 0.066 eV above the ground state, where the first one is the O-C-O bending and the second one is the C-C in plane wagging mode. DFT calculations in Ref.[49] revealed that the CH_2COOH radical is unstable by 0.03 eV and will most

ACCEPTED MANUSCRIPT
The Journal of Chemical Physics
AIP Publishing
This is the author's peer reviewed, accepted manuscript. However, the online version of record will be different from this version once it has been copyedited and typeset.
PLEASE CITE THIS ARTICLE AS DOI: 10.1063/5.0226252

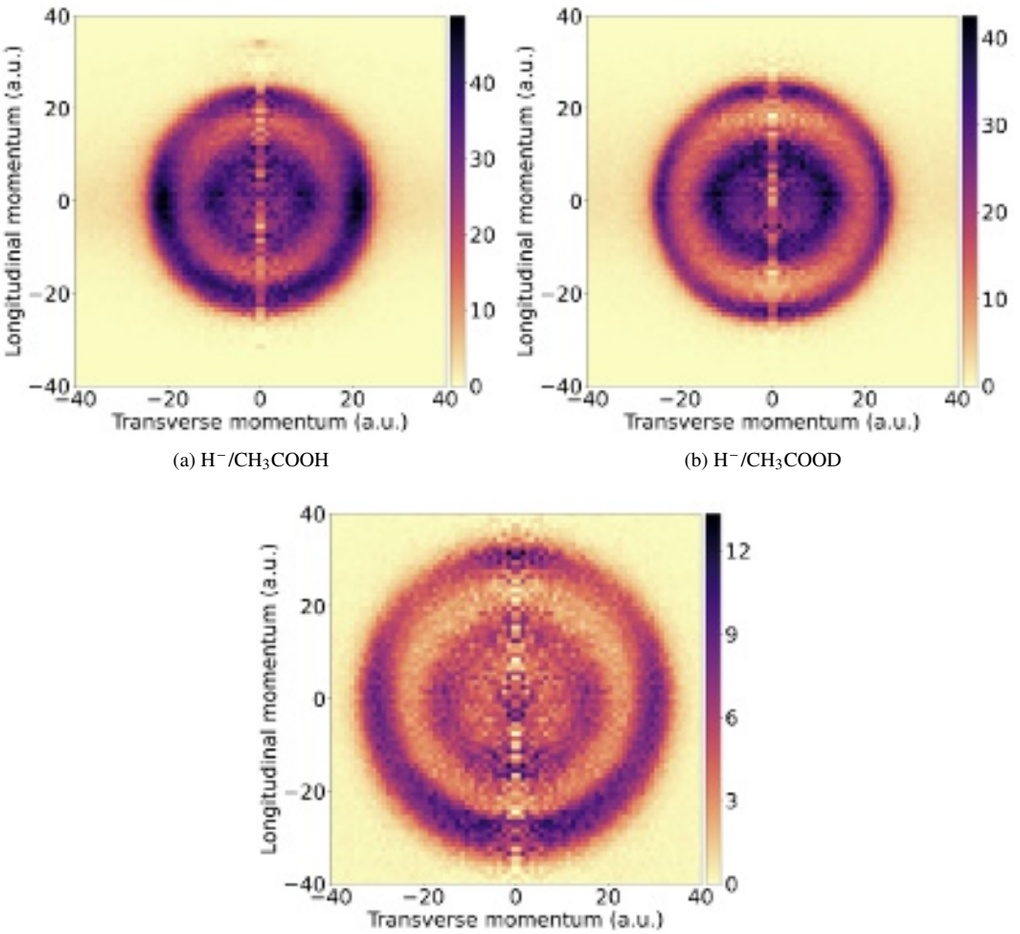

(a) H^-/CH_3COOH (b) H^-/CH_3COOD

(c) D^-/CD_3COOD

FIG. 5. Momentum distribution of H^- and D^- ions from C-H/C-D bond cleavage of CH_3COOH, CH_3COOD and CD_3COOD at 9.1 eV. The incident electron momentum is in the positive longitudinal direction (upward), and each color scale shows the ion yield in arbitrary units.

likely dissociate into the fragments CH_3 and CO_2.

In the present experiments, for O-H/O-D bond breakage at 6.7 eV and 7.7 eV, the energies available for excitation of the neutral CH_3COO radical are approximately 0.25 eV and 1 eV, respectively. Such low internal energies are consistent with two-body fragmentation (Reaction 1 in Tab. I), although several low-lying excited vibrational and electronic states are accessible at this energy. For the higher energy resonances at 9.1 eV and 10 eV, the energies partitioned into the neutral fragment are between 1.52 eV and 2.9 eV, suggesting a higher probability of isomerization and/or dissociation of metastable CH_3COO[15].

Turning to the C-H/C-D bond breakage, it is implausible that the slow H^-/D^- ions are the result of two-body dissociation, because the energy deposited in CH_2COOH, CH_2COOD, and CD_2COOD would be 4.63 eV, 4.41 eV, and 4.62 eV, respectively. Such high internal energy is sufficient for direct three-body dissociation, as represented by the dissociation Reaction 3 in Tab. I, with a thermodynamic threshold of 3.39 eV. The higher energetic thresholds of 5.46 eV and 7.99 eV (Reactions 4 and 5 in Tab. I) are also possible. In contrast, for the fast H^-/D^- ions at the same electron attachment energy, the internal energy of the neutral fragments are much lower, ranging from 1 eV to 3 eV, and the distribution is narrow. Therefore, we expect a prompt two-body fragmentation, where most of the available energy is partitioned into translational kinetic energy, although the metastable neutral radical may subsequently undergo further dissociation. The branching ratios of C-H/CH_3COOH and C-D/CD_3COOD breaks to produce fast and slow H^- and D^- anions are roughly the same. It is around 4:1, whereas for C-H/CH_3COOD break it is around 3:1.

The fits to the measured angular distributions (Figs 4 and 7) indicate that all four resonances, each corresponding to a distinct TNI state, have A' symmetry. However, due to their broad width of each resonance and their overlaps in energy, we do not rule out the possibility of A'' symmetry for the second and third resonances, because some of the A' character may be embedded by a nearby resonance into each of those angular distributions. We note that the broad resonance widths[11]

ACCEPTED MANUSCRIPT
The Journal of Chemical Physics
AIP Publishing
This is the author's peer reviewed, accepted manuscript. However, the online version of record will be different from this version once it has been copyedited and typeset.
PLEASE CITE THIS ARTICLE AS DOI: 10.1063/5.0226252

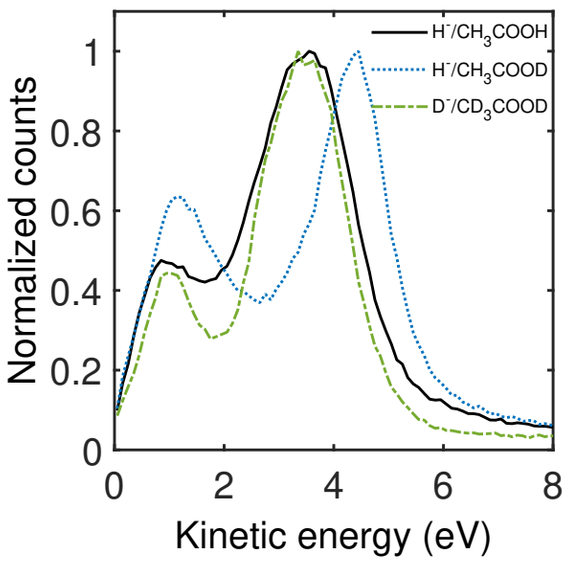

FIG. 6. Kinetic energy distribution of H^- and D^- ions from C-H/C-D bond cleavage of DEA to CH_3COOH, CH_3COOD, and CD_3COOD at incident electron energies of 9.1 eV. The ion yield for each distribution is rescaled to a maximum of 1 (arbitrary units).

are comparable to the present electron beam energy resolution of (0.5 eV), and the intrinsic energy width of each resonance is primarily due to the projection of the ground state of the neutral molecule in the Franck-Condon region onto the repulsive potential energy surface of each TNI state[50]. To characterize each TNI resonance, we consider the possible neutral parent states of the present Feshbach resonances from the VUV photoabsorption[10,51–56] and EEL[57] spectra in the literature. We turn our attention now to the O-H/O-D break at the 6.7 eV resonance. Leach *et al.*[10] have reported two transitions just above 6.7 eV: (i) the valence transition $13a' \rightarrow 14a'$ at 6.669 eV (calculated) with an oscillator strength of 0.047, and (ii) the Rydberg transition $13a' \rightarrow 3sa'$ at 7.25 eV (experimental) with an oscillator strength of 0.02. They assigned the valence transition $13a' \rightarrow 14a'$ as the $n_0' \rightarrow \sigma_{OH}'$ transition, which is the same as the $\tilde{A}' - X$ transition in the nomenclature of Bell *et al.*[51]. Robin[54] assigned the broad feature at 7.08 eV as an $n_0 \rightarrow 3s$ Rydberg transition. Ari *et al.*[57] assigned a feature in EELS at 7.1 eV to the $13a' \rightarrow 3sa'$ Rydberg transition, which appears to agree with Refs.[10,53,54]. Based on these studies, the valence state $(13a')^{-1}(14a')^1$ or Rydberg state $(13a')^{-1}(3sa')^1$ could be the parent TNI state of a Feshbach resonance. Therefore, in the 6.7 eV Feshbach resonance, the incident electron may excite the $13a'$ valence electron and be captured simultaneously either in the $14a'$ valence orbital or the $3sa'$ Rydberg orbital, giving the TNI state an A' symmetry. This indicates a possible mixed valence and Rydberg character in the first resonance.

The Rydberg optical transition to the 3s orbital in acetic acid shows a broad diffuse structure similar to the corresponding structure in formic acid[10,51]. The maximum of the band in acetic acid is at 7.795 eV[10]. Leach *et al.*[10] further identified three valence transitions in their VUV photoabsorption measurements and calculations, although they were found to be one order of magnitude weaker than the Rydberg transition. We note also that the EELS[57] investigation found a prominent peak at 7.8 eV, which was assigned to a $\pi \rightarrow \pi^*$ transition. Since the symmetry of the 7.7 eV resonance is most likely A' (Fig. 4b), the parent is probably either the Rydberg state $(13a')^{-1}(3sa')^1$, or a mixture of Rydberg and valence $(3a'')^{-1}(4a'')^1$, configurations.

We will now discuss 9.1 eV resonance, which dissociates by both O-H and C-H bond break. Three Rydberg bands, which are candidate parent TNI states of a Feshbach resonance at 9.1 eV, have been reported in spectroscopic studies[10,56] as the following transitions: (i) $13a' \rightarrow 3da'$ at 8.948 eV, (ii) $13a' \rightarrow 4sa'$ at 8.994 eV, and (iii) $3a'' \rightarrow 3pa''$ at 9.268 eV. The first A' Rydberg transition $13a' \rightarrow 3da'$ is a weak band. The second A' Rydberg transition $13a' \rightarrow 4sa'$ was reported in two EELS studies[56,57], where the corresponding band starts at 9.0 eV. It was assigned to a $n_0 \rightarrow 4s$ transition. We consider the $(13a')^{-1}(4sa')^1$ state could be the parent state of a Feshbach resonance at 9.1 eV, consistent with the A' symmetry, which is evident in Figs. 4c and 7.

The two distinct momentum rings we observe at 10 eV for O-H scission from CH_3COOD in Fig. 2d suggest two different pathways leading to different ion momenta. Previous measurements[11] of the D^- yield from O-D bond breakage in CH_3COOD[11] show only weak contributions between 9 eV and 10 eV that manifest as a high energy shoulder of the 7.7 eV resonance. To understand the possible origins of the two rings, we consider first the possibility that O-D scission produces the acetyloxyl radical in two low-lying electronic states[14,47]. It is possible that a conical intersection between two excited states of the neutral acetic acid in the third resonance leads to the two low-lying excited state of the acetyloxyl radical, analogous to the formyloxyl states produced by the A' resonance in formic acid[50]. The dependence of the relative yields of the two rings to the attachment energies above and below 10 eV suggests, however, that the inner ring is due to a contribution from the 9.1 eV resonance. We found that the inner ring yield decreases as the electron beam energy is increased above 9.1 eV, while the outer ring yield increases as the beam energy is increased from 9.1 eV and 10 eV.

We have not found any previous reports of the 10 eV TNI resonance observed as the outer ring in Fig. 2d. A corresponding parent neutral state could be populated by any of the following Rydberg transitions[10]: (i) $13a' \rightarrow 4pa'$ at 9.435 eV, (ii) $13a' \rightarrow 4da'$ at 9.695 eV, and (iii) $13a' \rightarrow 5sa'$ at 9.78 eV. Notably, the 10 eV resonance has around 1 eV higher KER than the 9 eV resonance, which suggests that both resonances produce acetyloxyl in the ground electronic state.

We now consider the effect of methylation on the DEA resonances and dynamics by a comparison between acetic acid and formic acid, which was studied previously by anion fragment momentum imaging[50]. In Fig. 8, we compare the angular distributions of H^- for O-H bond breakage at 7.25 eV and 7.7 eV for DCOOH and CH_3COOH, respectively. In CH_3COOH, we observe that the emission of the H^- frag-

ACCEPTED MANUSCRIPT
The Journal of Chemical Physics
AIP Publishing
This is the author's peer reviewed, accepted manuscript. However, the online version of record will be different from this version once it has been copyedited and typeset.
PLEASE CITE THIS ARTICLE AS DOI: 10.1063/5.0226252

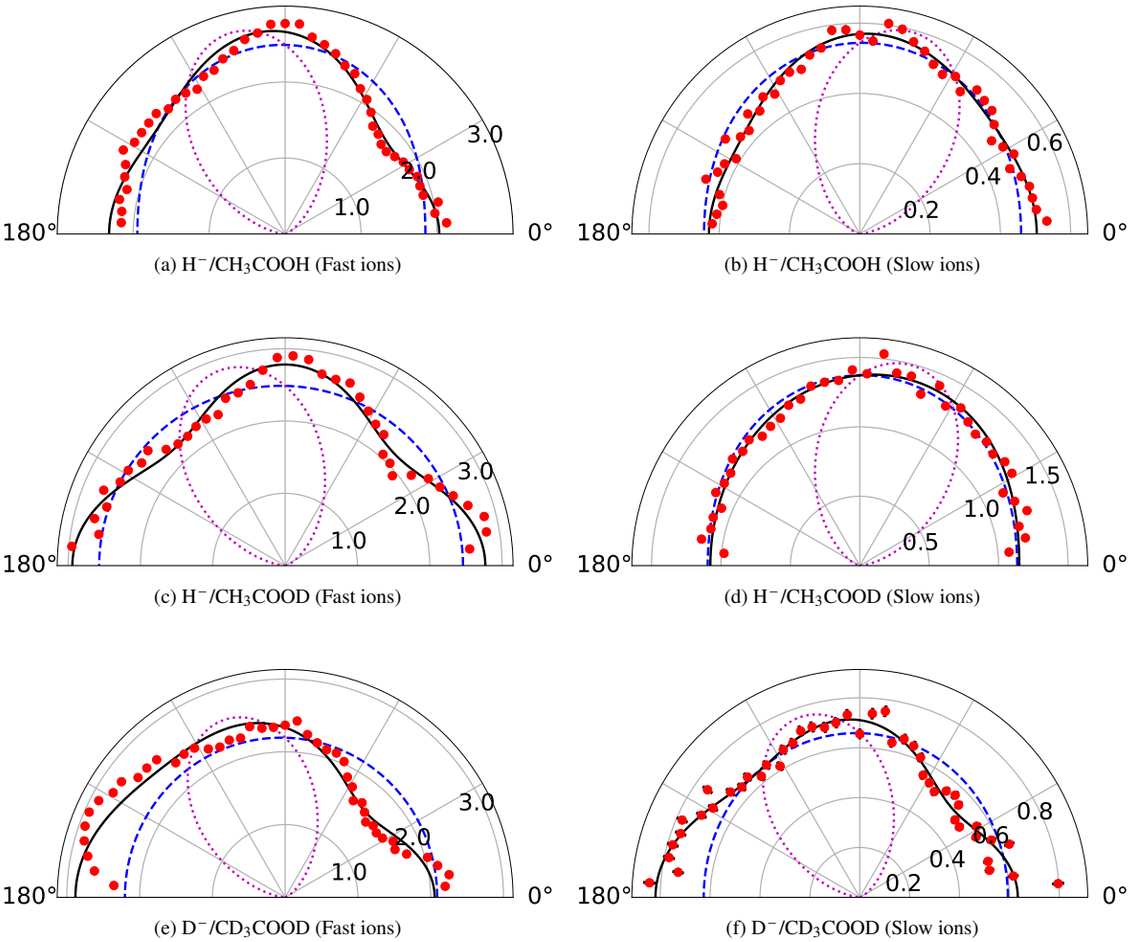

FIG. 7. Angular distribution of H^- (D^-) ions from C-H (C-D) bond cleavage of DEA to CH_3COOH, CH_3COOD, and CD_3COOD at 9.1 eV. The experimental angular distributions (solid red circle) are fitted with the assumption of a $A' \rightarrow A'$ transition using partial waves s+p (dashed blue line) and s+p+d (solid black line), and under the assumption of a $A' \rightarrow A''$ transition using p+d (dotted purple line). The incident electron direction is 0 deg,and the ion yields are displayed on a linear scale in arbitrary units.

ment mainly occurs in the backward direction near 180°. In contrast, the H^- from DCOOH is emitted mainly in the forward direction near 0°, i.e., in the direction of the electron beam. The squared modulus of the 3D entrance amplitude [50] (the electron attachment probability in the molecular frame) for O-H bond breakage from the lowest $^2A'$ Feshbach resonance in formic acid shows that electrons have a maximum probability for attaching to the molecule when the O-H direction is parallel to the incident electron beam direction (top sketch in Fig. 9). A similar comparison can be made for the 6.7 eV resonance in CD_3COOD with the 7.25 eV resonance in HCOOD. The general trend is that the angular distributions of H^- from CH_3COOH and DCOOH resemble mirror images of each other (Fig. 8). In acetic acid, the O−C=O equilibrium bond angle is 123°[10,59]. The electronic structure study in Ref.[14] has shown that, at their optimized geometries, the ground state of the acetyloxyl radical as well as the low-lying excited states all have C_s symmetry, and the O−C=O bond angles vary from $110-141°$, which suggests some rotation of the O-H bond is likely as the acetic acid TNI dissociates by O-H break. If such rotation is sufficiently small the the ARA is remains valid, and we find electron attachment probability is highest when the O-H bond is aligned antiparallel to the incident beam, as depicted in the bottom sketch of Fig. 9, in contrast with formic acid. This could possibly be confirmed by future *ab initio* electron scattering calculations.

VI. CONCLUSION

We have presented the results of the 3D anion momentum imaging measurements of DEA to acetic acid and its partially and fully deuterated forms, leading to H^-/D^- fragments from O-H/O-D and C-H/C-D bond scissions at four resonance energies spanning 6.7 eV to 10 eV. We also measured the kinetic energy and angular distributions of the H^- and D^- anions.

ACCEPTED MANUSCRIPT
The Journal of Chemical Physics
AIP Publishing
This is the author's peer reviewed, accepted manuscript. However, the online version of record will be different from this version once it has been copyedited and typeset.
PLEASE CITE THIS ARTICLE AS DOI: 10.1063/5.0226252

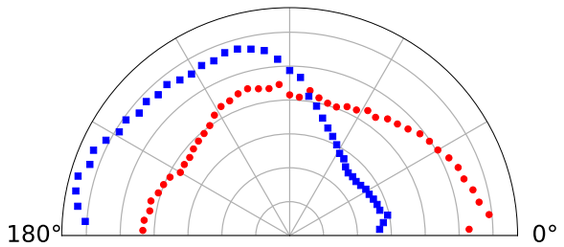

FIG. 8. Measured H^- angular distribution from O-H bond breakage for the 7.7 eV electron attachment resonance in acetic acid CH_3COOH (blue square) compared with the corresponding angular distribution at 7.25 eV in partially deuterated formic acid, DCOOH (red circle). The ion yields are displayed on a linear scale in arbitrary units.

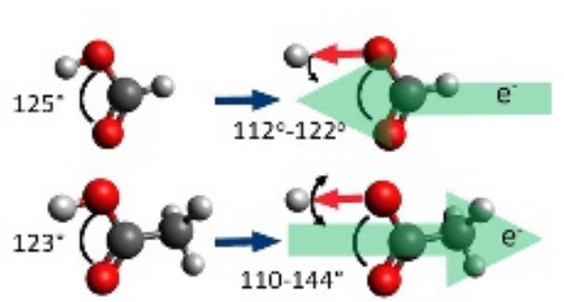

FIG. 9. Comparison of the maximum probability of attaching an electron to formic acid[50] and acetic acid. The red arrow represents the O-H dissociation axis. The green arrow indicates the preferred electron attachment direction for generating the measured angular distribution in Fig. 8. The O-C-O bond angles for the ground and low-lying electronic states are taken from[10,14,58].

The energy partitioning indicates mostly two-body dissociation for O-H/O-D bond breakage at all energies, whereas the C-H/C-D bond breakage at the 9.1 eV resonance indicates the involvement of both two- and three-body dissociation with a branching ratio of 4:1 for both CH_3COOH and CD_3COOD, and 3:1 for CH_3COOD. The anion fragment angular distributions were analyzed under the assumption that the axial recoil approximation holds, in order to determine the most likely symmetries of each TNI electronic state. The angular distributions are found to be consistent with all four resonances having A' symmetry. We note that, due to the energy-overlapping nature of these resonances, contributions from A'' symmetry, particularly above 7.7 eV, should not be ruled out. Both the 6.7 eV and 7.7 eV Feshbach resonances are tentatively assigned as having mixed valence and Rydberg character. By comparing the present experimental results with recent experimental and theoretical investigations of formic acid, we find that the 9.1 eV resonance proceeds via both O-H and C-H bond scission. For O-D bond breakage from CH_3COOD at 10 eV, where we observe two distinct D^- momentum rings, providing strong evidence for a fourth A' resonance that, to our knowledge, has not been previously reported. Finally, we conclude that electron attachment to acetic acid for all four resonances is generally most likely to take place in the molecular plane with the methyl functional group in the forward direction relative to the incident electron. This contrasts with the A' resonance in formic acid, where the electron attachment amplitude is highest when the hydroxyl functional group is in the forward direction.

ACKNOWLEDGMENTS

This work was supported by the US Department of Energy (DOE), Office of Science (Sc), Division of Chemical Sciences Geosciences and Biosciences (CSGB) of the Office of Basic Energy Sciences (BES) under Award No. DE-SC0019482. Work at LBNL was supported by DOE Sc BES CSGB under Award No. DE-AC02-05CH11231. We are indebted to the RoentDek Company for long-term support with detector software and hardware.

CONFLICTS OF INTEREST

The authors have no conflicts to disclose.

AUTHOR CONTRIBUTIONS

M.H., M.C. and D.S.S. designed the experiment. M.H., Th. W., and D.S.S. conducted the experiments. M.H. analyzed the data. M.H. and D.S.S. wrote the manuscript with significant review and editing by Th.W and M.C.. M.H. generated the figures.

DATA AVAILABILITY

The data-sets generated during the current study are available from the corresponding author upon reasonable request.

REFERENCES

[1]Pedatsur Neta, Miomir Simic, and Elie Hayon. Pulse radiolysis of aliphatic acids in aqueous solutions. i. simple monocarboxylic acids. *The Journal of Physical Chemistry*, 73(12):4207–4213, 1969. doi:10.1021/j100846a029.
[2]Oddur Ingólfsson. *Low-Energy Electrons: Fundamentals and Applications*. CRC Press, 2019.
[3]George J. Schulz. Resonances in electron impact on diatomic molecules. *Rev. Mod. Phys.*, 45:423–486, Jul 1973. doi:10.1103/RevModPhys.45.423.
[4]Wolfgang Sailer, Andrzej Pelc, Michael Probst, Jumras Limtrakul, Paul Scheier, Eugen Illenberger, and Tilmann D Märk. Dissociative electron attachment to acetic acid (ch3cooh). *Chemical Physics Letters*, 378(3): 250–256, 2003. doi:https://doi.org/10.1016/S0009-2614(03)01285-5.
[5]A. Pelc, W. Sailer, P. Scheier, N.J. Mason, E. Illenberger, and T.D. Märk. Electron attachment to simple organic acids. *Vacuum*, 70(2):429–433, 2003. doi:https://doi.org/10.1016/S0042-207X(02)00682-6. The International Symposium on Ion Implantation and Other Applica tions of Ions and Electrons - ION 2002.

ACCEPTED MANUSCRIPT
The Journal of Chemical Physics
AIP Publishing
This is the author's peer reviewed, accepted manuscript. However, the online version of record will be different from this version once it has been copyedited and typeset.
PLEASE CITE THIS ARTICLE AS DOI: 10.1063/5.0226252

[6]A. Pelc, W. Sailer, P. Scheier, and T.D. Märk. Generation of (m-h)- ions by dissociative electron attachment to simple organic acids. *Vacuum*, 78(2): 631–634, 2005. doi:https://doi.org/10.1016/j.vacuum.2005.01.099. Proceedings of the fifth International Conference on Ion Implantation and other Applications of Ions and Electrons (ION 2004).

[7]Dipayan Chakraborty, Giorgi Kharchilava, Ian Carmichael, and Sylwia Ptasinska. Dissociative electron attachment studies of gas-phase acetic acid using a velocity map imaging technique. *Journal of Physics B: Atomic, Molecular and Optical Physics*, 56(24):245202, jan 2024. doi: 10.1088/1361-6455/ad1745.

[8]Vaibhav S. Prabhudesai, Dhananjay Nandi, Aditya H. Kelkar, and E. Krishnakumar. Functional group dependent dissociative electron attachment to simple organic molecules. *The Journal of Chemical Physics*, 128(15): 154309, 04 2008. doi:10.1063/1.2899330.

[9]T. C. Freitas, M. T. do N. Varella, R. F. da Costa, M. A. P. Lima, and M. H. F. Bettega. Low-energy electron collisions with acetic acid. *Phys. Rev. A*, 79: 022706, Feb 2009. doi:10.1103/PhysRevA.79.022706.

[10]Sydney Leach, Martin Schwell, Sun Un, Hans-Werner Jochims, and Helmut Baumgärtel. Vuv absorption spectrum of acetic acid between 6 and 20ev. *Chemical Physics*, 321(1):159–170, 2006. doi: https://doi.org/10.1016/j.chemphys.2005.08.044.

[11]Vaibhav S. Prabhudesai, Aditya H. Kelkar, Dhananjay Nandi, and E. Krishnakumar. Functional group dependent site specific fragmentation of molecules by low energy electrons. *Phys. Rev. Lett.*, 95:143202, Sep 2005. doi:10.1103/PhysRevLett.95.143202.

[12]Vaibhav S Prabhudesai, N Bhargava Ram, G Aravind, P Rawat, and E Krishnakumar. Probing site selective fragmentation of molecules containing hydroxyl group using velocity slice imaging. *Journal of Physics: Conference Series*, 80(1):012016, sep 2007. doi:10.1088/1742-6596/80/1/012016.

[13]M. Bertin, D. Cáceres, M.P. Davis, R. Balog, A. Lafosse, N.J. Mason, E. Illenberger, and R. Azria. Electron stimulated desorption of h- ions from condensed acetic acid. *Chemical Physics Letters*, 433(4):292–295, 2007. doi:https://doi.org/10.1016/j.cplett.2006.11.052.

[14]Arvi Rauk, Dake Yu, and David A. Armstrong. Carboxyl free radicals: Formyloxyl (hcoo.bul.) and acetyloxyl (ch3coo.bul.) revisited. *Journal of the American Chemical Society*, 116(18):8222–8228, 1994. doi: 10.1021/ja00097a031.

[15]Zhou Lu and Robert E. Continetti. Dynamics of the acetyloxyl radical studied by dissociative photodetachment of the acetate anion. *The Journal of Physical Chemistry A*, 108(45):9962–9969, 2004. doi:10.1021/jp040355v.

[16]E. A. Lissi, G. Massiff, and A. E. Villa. Oxidation of carbon monoxide by methoxy-radicals. *J. Chem. Soc., Faraday Trans. 1*, 69:346–351, 1973. doi:10.1039/F19736900346.

[17]Baoshan Wang, Hua Hou, and Yueshu Gu. Ab initio/density functional theory and multichannel rrkm calculations for the ch3o + co reaction. *The Journal of Physical Chemistry A*, 103(40):8021–8029, 1999. doi: 10.1021/jp991203g.

[18]Prasad Ramesh Joshi, Kylie Chia-Yee How, and Yuan-Pern Lee. Hydrogen abstraction of acetic acid by hydrogen atom to form carboxymethyl radical •ch2c(o)oh in solid para-hydrogen and its implication in astrochemistry. *ACS Earth and Space Chemistry*, 5(1):106–117, 2021. doi: 10.1021/acsearthspacechem.0c00316.

[19]H. Adaniya, D. S. Slaughter, T. Osipov, T. Weber, and A. Belkacem. A momentum imaging microscope for dissociative electron attachment. *Review of Scientific Instruments*, 83(2):023106, 02 2012. doi:10.1063/1.3685244.

[20]P. J. Chantry and G. J. Schulz. Kinetic-energy distribution of negative ions formed by dissociative attachment and the measurement of the electron affinity of oxygen. *Phys. Rev.*, 156:134–141, Apr 1967. doi: 10.1103/PhysRev.156.134.

[21]R. J. Van Brunt and L. J. Kieffer. Angular distribution of O- from dissociative electron attachment to O2. *Physical Review A*, 2(5):1899–1905, November 1970. ISSN 0556-2791. doi:10.1103/PhysRevA.2.1899. URL `http://link.aps.org/doi/10.1103/PhysRevA.2.1899`.

[22]Hidehito Adaniya. *Imagining dissociation dynamics: Experimental study of electron attachment to water molecule by COLTRIMS technique*. PhD thesis, University of California, Davis, January 2009.

[23]D S Slaughter, H Adaniya, T N Rescigno, D J Haxton, A E Orel, C W McCurdy, and A Belkacem. Dissociative electron attachment to carbon dioxide via the 8.2 ev feshbach resonance. *Journal of Physics B: Atomic, Molecular and Optical Physics*, 44(20):205203, sep 2011. doi:10.1088/0953-4075/44/20/205203. URL `https://dx.doi.org/10.1088/0953-4075/44/20/205203`.

[24]EW Lemmon, MO McLinden, and DG Friend. Nist chemistry webbook (http://webbook. nist. gov); jd cox, dd wagman and va medvedev. *CODATA Key Values for Thermodynamics (http://www. codata. org)*.

[25]John L. Holmes, Fred P. Lossing, and Paul M. Mayer. Heats of formation of oxygen-containing organic free radicals from appearance energy measurements. *Journal of the American Chemical Society*, 113(26):9723–9728, 1991. doi:10.1021/ja00026a002.

[26]M W Chase. The journal of physical and chemical reference data. 2008.

[27]R. Yamdagni and P. Kebarle. Intrinsic acidities of carboxylic acids from gas-phase acid equilibriums. *Journal of the American Chemical Society*, 95 (12):4050–4052, 1973. doi:10.1021/ja00793a038.

[28]John Rumble et al. Crc handbook of chemistry and physics. 2017.

[29]Richard N. Zare. Dissociation of H2+ by Electron Impact: Calculated Angular Distribution. *The Journal of Chemical Physics*, 47(1):204–215, 07 1967. doi:10.1063/1.1711847.

[30]Thomas F. O'Malley and Howard S. Taylor. Angular dependence of scattering products in electron-molecule resonant excitation and in dissociative attachment. *Phys. Rev.*, 176:207–221, Dec 1968. doi: 10.1103/PhysRev.176.207.

[31]Daniel J. Haxton, C. William McCurdy, and Thomas N. Rescigno. Angular dependence of dissociative electron attachment to polyatomic molecules: Application to the $^2b_1$ metastable state of the h_2O and h_2S anions. *Phys. Rev. A*, 73:062724, Jun 2006. doi:10.1103/PhysRevA.73.062724.

[32]Gabriela C. G. Waschewsky, Phillip W. Kash, Tanya L. Myers, David C. Kitchen, and Laurie J. Butler. What woodward and hoffmann didn't tell us: the failure of the born–oppenheimer approximation in competing reaction pathways. *J. Chem. Soc., Faraday Trans.*, 90:1581–1598, 1994. doi: 10.1039/FT9949001581.

[33]Hyuk Kang, Boyong Jung, and Seong Keun Kim. Mechanism for ultrafast internal conversion of adenine. *The Journal of Chemical Physics*, 118(15): 6717–6719, 04 2003. doi:10.1063/1.1566438.

[34]D S Slaughter, A Belkacem, C W McCurdy, T N Rescigno, and D J Haxton. Ion-momentum imaging of dissociative attachment of electrons to molecules. *Journal of Physics B: Atomic, Molecular and Optical Physics*, 49(22):222001, oct 2016. doi:10.1088/0953-4075/49/22/222001.

[35]D. J Haxton, H. Adaniya, D. S Slaughter, B. Rudek, T. Osipov, T. Weber, T. N Rescigno, C. W McCurdy, and A. Belkacem. Observation of the dynamics leading to a conical intersection in dissociative electron attachment to water. *Phys. Rev. A*, 84:030701, Sep 2011. doi: 10.1103/PhysRevA.84.030701.

[36]R Azria, Y Le Coat, G Lefevre, and D Simon. Dissociative electron attachment on h2s: energy and angular distributions of h- ions. *Journal of Physics B: Atomic and Molecular Physics*, 12(4):679, feb 1979. doi:10.1088/0022-3700/12/4/016.

[37]M Tronc, C Schermann, R I Hall, and F Fiquet-Fayard. Differential cross sections and angular distributions of h- from dissociative electron attachment to h2 between 3.75 ev and 13 ev. *Journal of Physics B: Atomic and Molecular Physics*, 10(2):305, feb 1977. doi:10.1088/0022-3700/10/2/017.

[38]N. Bhargava Ram and E. Krishnakumar. Dissociative electron attachment to h2s probed by ion momentum imaging. *Phys. Chem. Chem. Phys.*, 13: 13621–13628, 2011. doi:10.1039/C1CP20642G.

[39]Krishnendu Gope, Nigel Mason, E. Krishnakumar, and Vaibhav S. Prabhudesai. Dea dynamics of chlorine dioxide probed by velocity slice imaging. *Phys. Chem. Chem. Phys.*, 21:14023–14032, 2019. doi: 10.1039/C8CP06660D.

[40]Dipayan Chakraborty, Aranya Giri, and Dhananjay Nandi. Dissociation dynamics in low energy electron attachment to ammonia using velocity slice imaging. *Phys. Chem. Chem. Phys.*, 21:21908–21917, 2019. doi: 10.1039/C9CP03973B.

[41]Pamir Nag, Michal Tarana, and Juraj Fedor. Effects of $\pi^*-\sigma^*$ coupling on dissociative-electron-attachment angular distributions in vinyl, allyl, and benzyl chloride and in chlorobenzene. *Phys. Rev. A*, 103:032830, Mar 2021. doi:10.1103/PhysRevA.103.032830.

[42]Dipayan Chakraborty, Daniel S. Slaughter, and Sylwia Ptasinska. Dynamics of resonant low-energy electron attachment to ethanol-producing hydroxide anions. *Phys. Rev. A*, 108:052806, Nov 2023. doi: 10.1103/PhysRevA.108.052806.

ACCEPTED MANUSCRIPT
The Journal of Chemical Physics
AIP Publishing
This is the author's peer reviewed, accepted manuscript. However, the online version of record will be different from this version once it has been copyedited and typeset.
PLEASE CITE THIS ARTICLE AS DOI: 10.1063/5.0226252

[43]J Fedor, P Cicman, B Coupier, S Feil, M Winkler, K Głuch, J Husarik, D Jaksch, B Farizon, N J Mason, P Scheier, and T D Märk. Fragmentation of transient water anions following low-energy electron capture by h2o/d2o. *Journal of Physics B: Atomic, Molecular and Optical Physics*, 39(18):3935, sep 2006. doi:10.1088/0953-4075/39/18/022.

[44]Prashant Rawat, Vaibhav S Prabhudesai, G Aravind, M A Rahman, and E Krishnakumar. Absolute cross sections for dissociative electron attachment to h2o and d2o. *Journal of Physics B: Atomic, Molecular and Optical Physics*, 40(24):4625, nov 2007. doi:10.1088/0953-4075/40/24/007.

[45]Martina Kieninger, Oscar N. Ventura, and Sandor Suhai. Density functional investigations of carboxyl free radicals: Formyloxyl, acetyloxyl, and benzoyloxyl radicals. *International Journal of Quantum Chemistry*, 70(2):253–267, 1998. doi:https://doi.org/10.1002/(SICI)1097-461X(1998)70:2<253::AID-QUA2>3.0.CO;2-T.

[46]Paul G. Wenthold and Robert R. Squires. Gas-phase properties and reactivity of the acetate radical anion. determination of the c-h bond strengths in acetic acid and acetate ion. *Journal of the American Chemical Society*, 116 (26):11890–11897, 1994. doi:10.1021/ja00105a032.

[47]Xue-Bin Wang, Hin-Koon Woo, Lai-Sheng Wang, Babak Minofar, and Pavel Jungwirth. Determination of the electron affinity of the acetyloxyl radical (ch3coo) by low-temperature anion photoelectron spectroscopy and ab initio calculations. *The Journal of Physical Chemistry A*, 110(15):5047–5050, 2006. doi:10.1021/jp060138p. PMID: 16610823.

[48]Dao-Ling Huang, Guo-Zhu Zhu, and Lai-Sheng Wang. Communication: Observation of dipole-bound state and high-resolution photoelectron imaging of cold acetate anions. *The Journal of Chemical Physics*, 142(9): 091103, 03 2015. doi:10.1063/1.4913924.

[49]Jean Ann Wyer, Linda Feketeová, Steen Brøndsted Nielsen, and Richard A J O'Hair. Gas phase fragmentation of protonated betaine and its clusters. *Physical chemistry chemical physics.*, 11(39), 2009.

[50]D. S. Slaughter, Th. Weber, A. Belkacem, C. S. Trevisan, R. R. Lucchese, C. W. McCurdy, and T. N. Rescigno. Selective bond-breaking in formic acid by dissociative electron attachment. *Phys. Chem. Chem. Phys.*, 22: 13893–13902, 2020. doi:10.1039/D0CP01522A.

[51]Stephen Bell, T. L. Ng, and A. D. Walsh. Vacuum ultra-violet spectra of formic and acetic acids. *J. Chem. Soc., Faraday Trans. 2*, 71:393–401, 1975. doi:10.1039/F29757100393.

[52]Masako Suto, Xiuyan Wang, and L. C. Lee. Fluorescence yields from photodissociative excitation of formic acid, methyl formate, and acetic acid in the vacuum-ultraviolet region. *The Journal of Physical Chemistry*, 92(13): 3764–3768, 1988. doi:10.1021/j100324a015.

[53]Edwin E. Barnes and William T. Simpson. Correlations among Electronic Transitions for Carbonyl and for Carboxyl in the Vacuum Ultraviolet. *The Journal of Chemical Physics*, 39(3):670–675, 08 1963. doi: 10.1063/1.1734305.

[54]Melvin Robin. *Higher Excited States of Polyatomic Molecules V3*, volume 3. Elsevier, 2012.

[55]S. Nagakura, K. Kaya, and H. Tsubomura. Vacuum ultraviolet absorption spectra and electronic structures of formic acid, acetic acid and ethyl acetate. *Journal of Molecular Spectroscopy*, 13(1):1–8, 1964. doi: https://doi.org/10.1016/0022-2852(64)90049-9.

[56]P. Limão-Vieira, A. Giuliani, J. Delwiche, R. Parafita, R. Mota, D. Duflot, J.-P. Flament, E. Drage, P. Cahillane, N.J. Mason, S.V. Hoffmann, and M.-J. Hubin-Franskin. Acetic acid electronic state spectroscopy by high-resolution vacuum ultraviolet photo-absorption, electron impact, He(I) photoelectron spectroscopy and ab initio calculations. *Chemical Physics*, 324 (2-3):339–349, May 2006. doi:10.1016/j.chemphys.2005.10.032.

[57]Tayfun Ari and M Haluk Güven. Valence–shell electron energy-loss spectra of formic acid and acetic acid. *Journal of Electron Spectroscopy and Related Phenomena*, 106(1):29–35, 2000. doi:https://doi.org/10.1016/S0368-2048(99)00084-5.

[58]R.Wellington Davis, A.G. Robiette, M.C.L. Gerry, E. Bjarnov, and G. Winnewisser. Microwave spectra and centrifugal distortion constants of formic acid containing 13c and 18o: Refinement of the harmonic force field and the molecular structure. *Journal of Molecular Spectroscopy*, 81(1):93–109, 1980. doi:https://doi.org/10.1016/0022-2852(80)90331-8.

[59]J.L. Derissen. A reinvestigation of the molecular structure of acetic acid monomer and dimer by gas electron diffraction. *Journal of Molecular Structure*, 7(1):67–80, 1971. doi:https://doi.org/10.1016/0022-2860(71)90008-1.